Mask Enhancement Using an Evanescent Wave Effect

Neal V. Lafferty†, Jianming Zhou, Bruce W. Smith
Center for Nanolithography Research
Rochester Institute of Technology, 82 Lomb Memorial Drive, Rochester NY 14623, USA

ABSTRACT

State of the art lithography is continually driven to resolve increasingly smaller features, forcing k_1 values for lithography processes ever lower. In order to image these difficult features with reliable fidelity, lithographers must increasingly use Resolution Enhancement Techniques (RETs). One such technique that is proposed in this paper uses small, sub-wavelength grooves placed in close proximity to an aperture. These sub-wavelength grooves create evanescent fields bound to the surface between the absorber and the mask substrate, decaying exponentially in lateral directions. In this work we demonstrate the ability to use such Evanescent Wave Assist Features[1] (EWAFs) to enhance the propagating near and far field energy within openings such as slits and contacts. Using a Finite Difference Time Domain model, the effects of these evanescent wave assist features are explored in both the near and far field regions. Several cases of absorber material, feature type, spacing, and illumination will be presented.

Keywords: Evanescent Wave, Resolution Enhancement Techniques, Composite Diffracted Evanescent Wave, CDEW, Evanescent Wave Assist Feature, EWAF

1. INTRODUCTION

Evanescent is used to describe something "that quickly vanishes or passes away; having no permanence"[2]. These mysterious fields were first discovered by Sir Isaac Newton but were not widely understood until many years later. Recently, the novel application of evanescent waves to optical lithography has become a subject of interest[1].

1.1. Mathematical Representation of the evanescent wave

Evanescent waves can be generated in a variety of ways, including Total Internal Reflection (TIR)[1,3]. As a beam at TIR approaches an interface to a lower index medium, all of its energy must be reflected back. Due to boundary conditions of the interface, however, some part of the field must still be transmitted. An evanescent field is transmitted through this interface, and is confined to the material surface. Since, on average, the evanescent field carries no energy across the boundary, both conditions are satisfied[3].

The mathematical form of the wave is described in equation (1). The transmitted electric field, E_{0t} is modulated by an exponential. The phase of the wave varies as it propagates in the x direction (in this case), while its amplitude varies along the y direction, hence the term inhomogeneous.

$$\vec{E}_t = \vec{E}_{0t} e^{\mp \beta y} e^{i(k_t x \sin\theta_i / n_{ti} - \omega t)} \tag{1}$$

If another optically dense medium is brought within several wavelengths of the first, in the region where the evanescent field exists, the disturbance can be frustrated and coupled into the second medium. This phenomenon is used extensively in the field of fiber optics and photonics, such as in waveguide-to-waveguide couplers[4].

1.2. Evanescent field of sub-wavelength features

Evanescent fields may also be generated through the use of sub-wavelength features. Of particular significance is the interaction of the evanescent field with propagating modes of radiation. Similar to the frustration of total internal reflection, the evanescent wave cannot be measured directly and therefore indirect methods must used. Leviatan et al., has demonstrated that sub-wavelength apertures with small

† N.V.L. E-mail: nxl7930@microe.rit.edu; Web: http://www.rit.edu/lithography

displacements relative to each other can indeed generate evanescent fields and couple the inhomogeneous field back to propagating modes[5]. Researchers have also demonstrated the use of evanescent fields in enhancing transmission through apertures on a screen[6]. More precisely, they have suggested the direct interference of the evanescent modes generated by an array of sub-wavelength features and propagating modes traveling through an aperture as a mechanism for enhancement and inhibition of intensity at that aperture[6]. Although there are similarities between this Composite Diffracted Evanescent Wave (CDEW) and the surface wave generated by TIR, the CDEW has the additional character of decaying in the lateral directions by *1/x*.[6] The CDEW can be supported in materials that are non-conductive, differentiating it from the effects caused by surface plasmon polaritons. The model for this enhancement can be seen in equation (2), where λ is the wavelength of light, α is the evanescent wave amplitude relative to the incident light amplitude, n_{eff} is the effective refractive index the evanescent wave experiences, and P is the pitch of the sub-wavelength grooves.

$$A(\lambda) = \left(1 + 2\sum_{j=1}^{N} \frac{\alpha d}{jP} \cos\left(\frac{2\pi}{\lambda} n_{eff}\, jP + \frac{\pi}{2}\right)\right)^2 \tag{2}$$

The sub-wavelength grooves have been referred to as Evanescent Wave Assist Features, or EWAFs, since their primary purpose in the lithographic scope is to "assist" the aperture which they surround[1]. Previous work has demonstrated that these gratings, buried under the mask absorber, have the ability to enhance or inhibit the intensity at the center of a slit or contact.

2. EVANESCENT WAVE ENHANCEMENT EFFECT

Prior work with EWAFs has focused on near-field enhancement of intensity at an aperture[1]. Expanding on these ideas, the enhancement effect is investigated more thoroughly and propagated to the far field. Analysis was performed on both the near-field effects (within several λ of the bottom of the mask), as well as in the far-field (in the object conjugate plane of a lithographic exposure system). Rigorous Finite Difference Time Domain (FDTD) software was used to perform all simulations[7]. An isotropic grid size of 5 nm was used for all simulations. Unless otherwise noted, analysis was performed for masks with uniform absorber materials. The refractive indices and approximate thicknesses of these materials are shown in Table 1.

Material	n	k	Thickness *(nm)*
Fused Silica	1.5631	0.0000	Varies
Chrome, Cr	0.8418	1.6472	90
Chrome Oxide, Cr_2O_3	1.6364	0.6504	90
Chrome Nitride, CrN	1.2921	0.8989	90

Table 1: Optical properties and thicknesses of materials used for simulation. All indices are given for λ*=193 nm*.

2.1. Near-Field Enhancement

Evanescent wave assist features were first considered for the case of a 45nm trench at 1X (1-D) and a Cr absorber layer. For the initial experiments, trench pitch was kept constant at 215 nm 1X, while the number of assist features between trenches was varied from 0 to 5. TE polarized illumination was used. This effectively varies the EWAF pitch and proximity to trenches while holding the main feature pitch constant. A sample reticle layout can be seen in Figure 1. For these simulations the EWAF depth was constrained to $\lambda/2n_{glass}$, which in this case corresponds to approximately 62 nm. For simplicity, n_{glass} will be represented by n throughout this paper. The near-field aerial images for 5 cases were compared across a cutline located in the center of the trench. The aerial images and cutline used to obtain them can be seen in Figure 1. The aerial images show a best case improvement when there are two assist features evenly spaced between neighboring trenches. In this best case, there is a 17% increase in intensity relative to the unassisted case, and a 20% decrease in trench width at the 0.75 level[1].

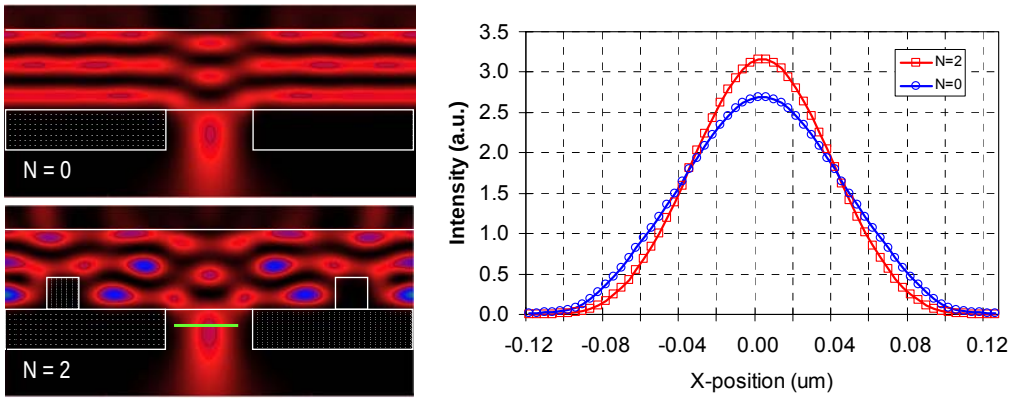

Figure 1: Near-field aerial images obtained from FDTD simulation. At this cutline, best case image enhancement occurs when two assist features are used between trenches. Compared to the unassisted trench, this corresponds to a 17% intensity increase and a 20% width decrease at the 0.75 level[1].

The EWAF pitch associated with the N=2 case is 247 nm. These results show that the assist features influence the intensity at the center of a trench. While these simulations show enhancement at the center of the contact, far-field simulations will require a shifted output plane location in order to accurately use the output of the mask simulation as an input to far-field optical simulation. Following established best simulation practices, the output plane was moved $\lambda/4$ below the lowest absorber surface and $\lambda/4$ above the bottom limit of the simulation domain[8].

A similar set of conditions was simulated in 2-D using TE illumination and multiple main feature duty ratios along with different numbers of assist features. In this scenario, a 45nm (1X) contact was flanked in X and Y dimensions with EWAFs as in Figure 2. Assist geometries were restricted to Manhattan style layouts in order to simplify simulation, however several alternative EWAF layouts and CDEW generating structures have been proposed in literature[1,6].

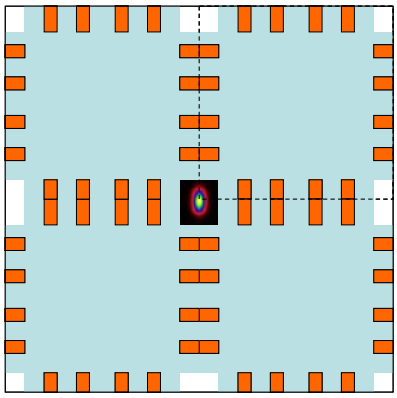

Figure 2: Simulation domain top-down view showing mask geometries. A single domain is outlined in dashed lines. The domains are arrayed in continuous infinite fashion. Since intensity at contact center is desired, the pattern is shifted to facilitate aerial image extraction and comparison at contact center. For the illustrated case, N=4.

Duty ratios investigated varied from 1:1.5 through 1:5.7 l/s. Since the main feature pitch was varied, the simulation domain was modified to place the center of each contact in a corner of the domain. Figure 2 shows the arrayed simulation domains and reconstruction of the intended contact, flanked by EWAFs.

Each duty ratio was simulated over multiple numbers of EWAFs, ranging from 0, the reference condition, to 5 EWAFs, space permitting. Results of the analysis indicate that the best performance of the EWAFs is achieved when the main feature pitch is selected such that the EWAF pitch is λ/n. A main feature pitch of 215 nm (1X) was selected to allow for such EWAF spacing to exist on mask with N=5 assists present. Constraining the width of the EWAF notches in glass to $\lambda/2n$, this leaves a 1:1 EWAF grating. This EWAF pitch agrees with grating pitch used in literature for surface wave generation in grating couplers[9].

Multiple mask absorber materials were investigated, such as CrN, TaN, and Cr_2O_3. These materials are shown in an index scatter plot in Figure 3. The influence of mask absorber material was also studied in conjunction with the feature depth. Figure 4 shows the results of these experiments.

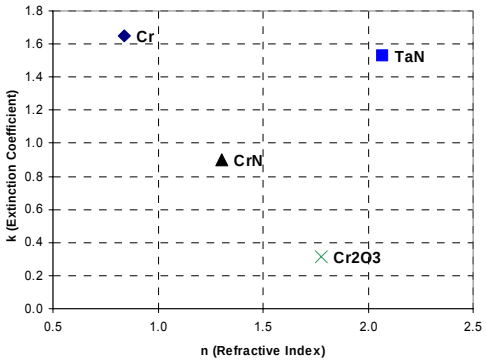

Figure 3: Scatter plot of extinction coefficient vs. refractive index for several convenient photomask absorber materials. CrN and Cr_2O_3 both exhibit unique enhancement effects.

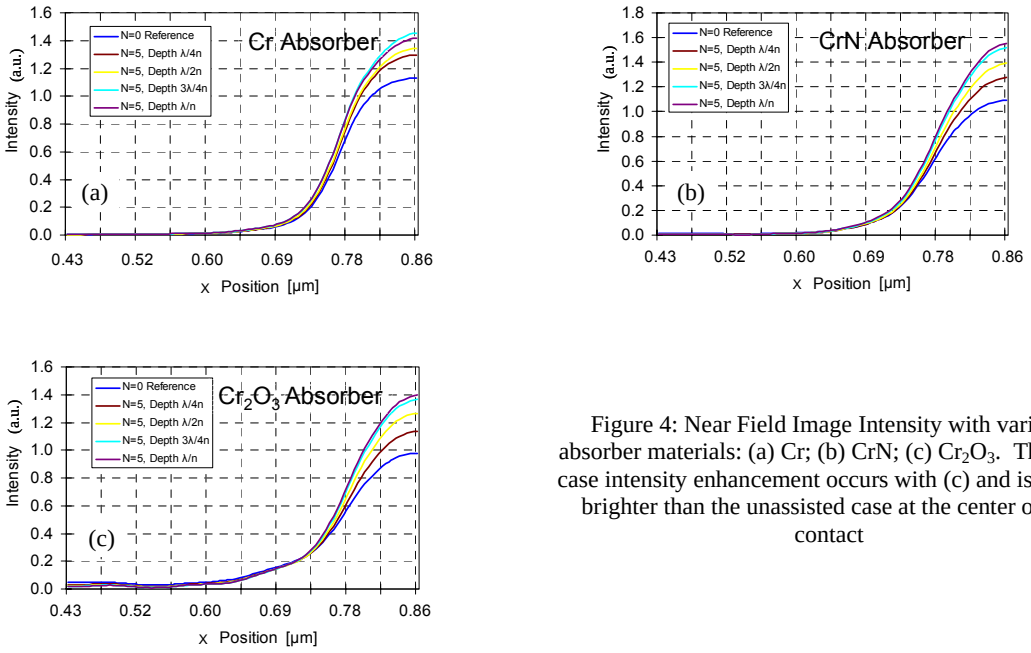

Figure 4: Near Field Image Intensity with various absorber materials: (a) Cr; (b) CrN; (c) Cr_2O_3. The Best case intensity enhancement occurs with (c) and is 42.6% brighter than the unassisted case at the center of the contact

Using the optimized main feature pitch and N=5 assist features, varying their depth from *λ/4n* to *λ/n* in increments of *λ/4n*, a best case intensity enhancement of 42.6% was achieved over the standard unassisted mask with a Cr_2O_3 absorber. This enhancement occurs at an EWAF depth of *λ/n*. Similarly, a 42% near-field intensity enhancement was achieved using CrN as a mask absorber material, coinciding with an EWAF depth of *λ/n*. The standard Cr absorber used for initial investigation showed a best case enhancement of 28.4 % at *3λ/4n* EWAF depth. Given the large intensity enhancement for Cr_2O_3, this material was selected for further experiments in the far field.

2.2. Far-Field Enhancement

Far field enhancement due to EWAF features was simulated using a dry 193 nm exposure tool with an NA of 0.93 and reduction ratio of 4X. Conventional illumination with a σ of 0.3 was used in combination with unpolarized, radial, and azimuthal input polarization. As mentioned in the previous section, the best case

Cr_2O_3 absorber mask with 45 nm (1X) contacts, main feature pitch of 215 nm (1X), and N=5 assist features was used as input for the far-field simulations.

2.2.1. Comparison of Diffracted Orders

In order to characterize the effect of the assist features in the far field, the diffracted orders were compared between cases of varying EWAF depth. The results are summarized in Figure 5.

Figure 5a shows that as EWAFs are added and depth is increased, 0^{th} order magnitude under TE polarization reduces by approximately 30% from the case of no EWAFs to the best case depth of λ/n. The $\pm1^{st}$ and $\pm2^{nd}$ orders also increase by approximately 20%. In Figure 5b, which is TM polarized, as EWAF depth is increased to the optimal λ/n, the $\pm1^{st}$ and $\pm2^{nd}$ orders also undergo a similar improvement.

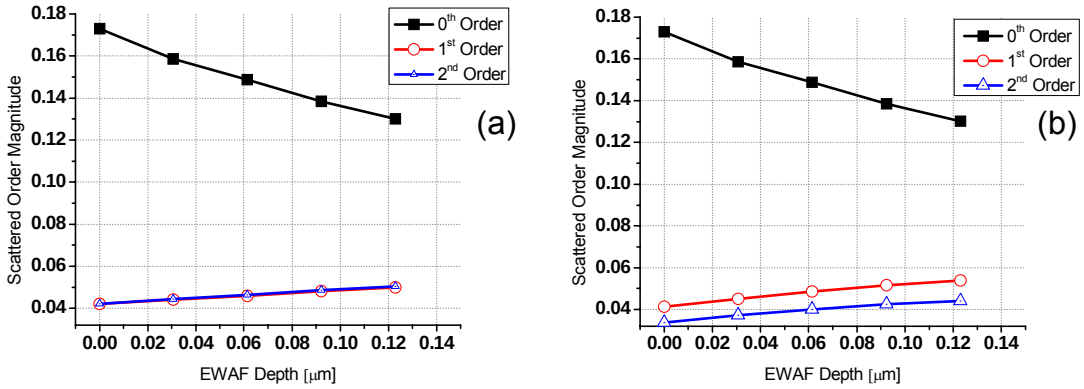

Figure 5: Scattered orders collected from a photomask (Cr_2O_3 absorber) containing EWAF structures. (a) indicates order magnitudes from TE polarization; (b) indicates order magnitudes from TM polarization.

2.2.2. Far field Aerial Image

Two dimensional aerial images for the cases simulated previously are shown in Figure 6. As expected from the analysis, images appear "darker" due to the loss of 0^{th} order intensity caused by the addition of EWAFs.

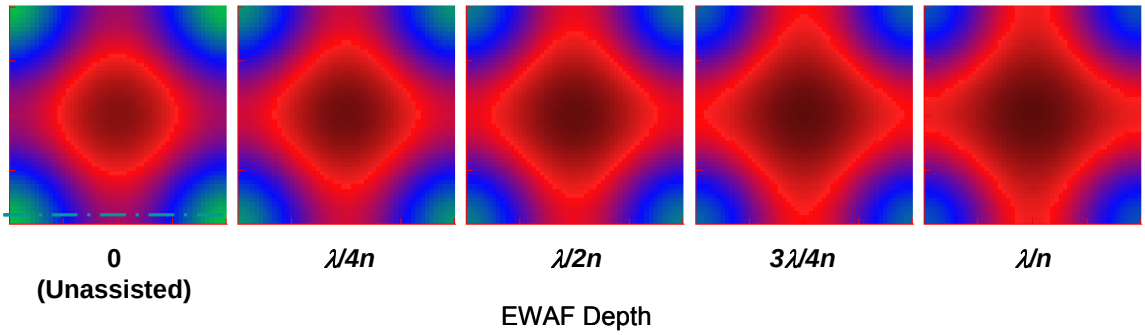

Figure 6: Far field aerial image with increasing EWAF depth. The line indicated in the unassisted case is used for cutlines to further compare images.

The cutline indicated in the unassisted aerial image of Figure 6 is used to gain a more meaningful understanding of the effects on aerial image in the far field. Figure 7 shows the aerial image comparison for unpolarized illumination.

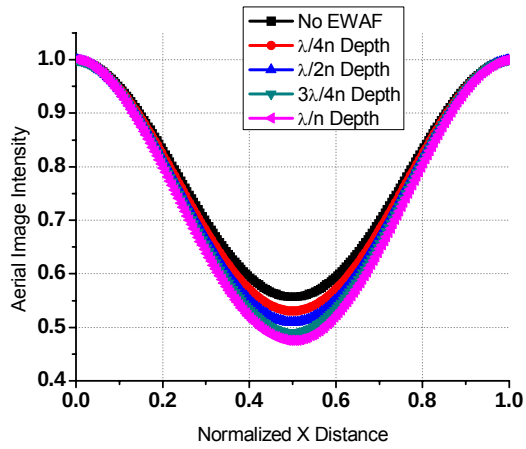

Figure 7: Comparison of x-cutline of unpolarized aerial images across EWAF depth. Best case contrast enhancement is 27%.

In order to remove the effects of the reduction in 0^{th} order and better visualize the effects of the increase in 1^{st} order, the data has been normalized to the intensity at contact center. The addition of the assist features in this case results in a contrast enhancement of 27% between the unassisted case and the case where λ/n depth EWAFs are used.

The experiment was repeated using radially and azimuthally polarized illumination. The use of radial polarization results in a lower contrast enhancement of 8% between unassisted and optimized EWAFs on reticle. Azimuthal illumination results in an unusual effect, whereby sidelobe-type artifacts are evident in the aerial image. In this case, contrast enhancements are difficult to quantify, since the formation of the lobes are undesired and magnified by the EWAFs. The results of the studies using radial and azimuthal polarization can be seen in Figure 8 and Figure 9.

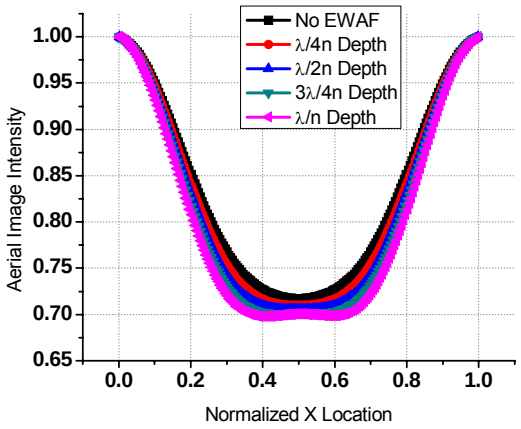

Figure 8: Comparison of x-cutline of radially polarized aerial images across EWAF depth. Best case contrast enhancement is 8%.

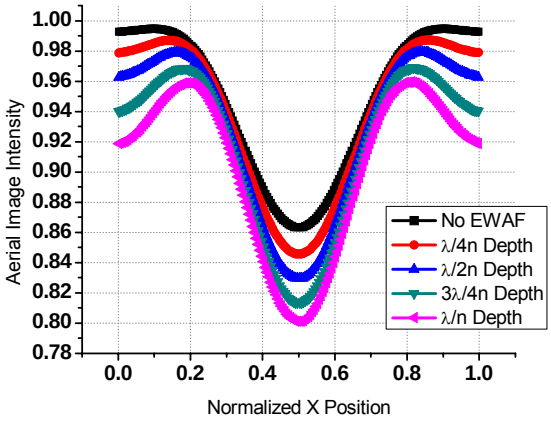

Figure 9: Comparison of x-cutline of azimuthally polarized aerial images across EWAF depth.

3. CONCLUSION

We have extended our investigation of Evanescent Wave Assist Features (EWAFs) to include both the near and far-field. In the near-field region, the technique primarily causes an increase in intensity in the center of an aperture surrounded by the assist features. Using TEMPEST pr2[7], we have modeled several different combinations of mask materials, number of assist features, assist feature depths, and main feature pitches. We report a best case enhancement in the near field intensity of 42.6% for the case of a 45nm (1X) contact at 215nm (1X) pitch using 5 EWAFs and Cr_2O_3 absorber material. A similar enhancement was also observed using CrN as an absorber (42% I gain). Far -field enhancement was simulated using a 0.93NA, 0.3σ (conventional) configuration. In the far-field region, we report a contrast enhancement of up to 20% using unpolarized light in conjunction with Cr_2O_3 mask absorber material.

ACKNOWLEDGEMENTS

The authors would like to acknowledge the support of SRC, Intel and Panoramic Technology.

REFERENCES

1. B. W. Smith, "Evanescent Wave Imaging in Optical Lithography" Proceedings of SPIE--the International Society for Optical Engineering (SPIE--the International Society for Optical Engineering, Bellingham, Wash., 2006)**, 6154,** 61540.

2. "Evanescent", *Oxford English Dictionary*, (Oxford University Press, Oxford; New York, N.Y., 1989).

3. E. Hecht, "Optics," in "Optics," in (Addison-Wesley, Reading, Mass., 1998) pp. 121.

4. G. T. Reed and A. P. Knights, "A Selection of Photonic Devices," in *Silicon Photonics :An Introduction*, "A Selection of Photonic Devices," (John Wiley & Sons, Chichester; Hoboken, NJ, 2004) pp. 172.

5. Y. Leviatan, "ELECTROMAGNETIC COUPLING BETWEEN TWO HALF-SPACE REGIONS SEPARATED BY TWO SLOT-PERFORATED PARALLEL CONDUCTING SCREENS." IEEE Transactions on Microwave Theory and Techniques (Professional Technical Group on Microwave Theory and Techniques, Institute of Electrical and Electronics Engineers, New York, N.Y., 1988)**, 36,** 44.

6. H. J. Lezec and T. Thio, "Diffracted Evanescent Wave Model for Enhanced and Suppressed Optical Transmission through Subwavelength Hole Arrays" Optics Express (Optical Society of America, Washington, DC, 2004)**, 12**.

7. T. V. Pistor, Panoramic Technology EM-Suite, Berkeley, CA, 2007.

8. T. V. Pistor, "EM-Suite Users Manual," 1, (2007), http://www.panoramictechnology.com/~support/.

9. G. T. Reed and A. P. Knights, "Silicon on Insulator Photonics," in *Silicon Photonics :An Introduction*, "Silicon on Insulator Photonics," in (John Wiley & Sons, Chichester; Hoboken, NJ, 2004) pp. 78.